# Removing Antenna Effects using an Invertible Neural Network for Improved Estimation of Multilayered Tissue Profiles using UWB Radar

Yuyi Chang, Nithin Sugavanam, and Emre Ertin The Ohio State University, Columbus, OH 43210, USA (chang.1560@osu.edu)

Abstract—Ultrawideband (UWB) radar sensors are an emerging biosensing modality that can be used to assess the dielectric properties of internal tissues. Antenna effects, including antenna body interactions limit the sensors ability to isolate the weak returns from the internal tissues. In this paper we develop a data driven calibration method for recovering Green's function of the multilayered media model of the tissue profiles using an Invertible Neural Network (INN). The proposed INN structure is trained to invert the antenna transfer function to form estimates of the Green's function modeling returns from internal tissues. We use simulation experiments to assess the effectiveness of the trained INN in antenna transfer function inversion.

#### I. Introduction

Ultrawideband (UWB) radar sensor is an emerging biosensing modality that provides a viable and noninvasive alternative for monitoring changes in internal tissue profiles indicative of chronic and acute disease states such as peripheral and pulmonary edema [1]. However, antenna effects, including antenna body interactions limit the sensors ability to isolate the weak returns from the internal tissues. Therefore, effective calibration methods are required to recover the underlying forward propagation model (i.e., Green's function) of the multilayered tissue profiles through estimating and inversion of antenna transfer function. Existing calibration methods typically use nonlinear optimization approaches to estimate the antenna transfer function from controlled measurements in the far field setting [2], [3]. In typical bio-sensing applications the sensor operates in close proximity of the body and therefore need to be calibrated in situ.

In this paper, we present an antenna calibration methodology to recover multilayered media Green's function using an Invertible Neural Network (INN) from training data collected in situ. We use simulation experiments to assess the effectiveness of the trained INN in antenna transfer function inversion.

#### II. PROPAGATION MODEL AND GREEN'S FUNCTION

# A. Antenna Propagation Model

In this paper, following [2], we consider the following antenna model for the observed frequency-domain measurements  $S_{12}(\omega)$ , with frequency dependent factors to model direct coupling, transmit and receive components.

$$S_{12}(\omega) = H_i(\omega) + H_t(\omega)G_{xx}(\omega)H_r(\omega) \tag{1}$$

where  $\omega$  represents the frequency,  $G_{xx}(\omega)$  is the Green's function for the multilayered media;  $H_i(\omega)$ ,  $H_t(\omega)$ , and  $H_r(\omega)$  represent return, transmitting, and receiving losses of

the antenna, respectively. The expression can be simplified by combining  $H_t(\omega)$  and  $H_r(\omega)$  as  $H(\omega)$ .

#### B. Green's Function of Multilayered Media

We consider a simplified forward propagation model under plane-wave assumption where the Green's function of the multilayered media is represented by the Riccati equations parameterized by local reflection coefficients. The full derivation of the Green's function can be found in [4].

#### C. Dataset

A synthetic dataset is created containing time domain passband  $G_{xx}(\omega)$  and associated  $S_{12}(\omega)$  based on equation (1). To obtain realistic values for  $H_i(\omega)$  and  $H(\omega)$  to use in our simulation experiments, we made measurements against stacked layers of Rogers Corporation TMM Laminates with known permittivity profiles using a Keysight N5242A VNA configured for step frequency measurements in the range of 0.5 - 6.0 GHz at 50 MHz steps.

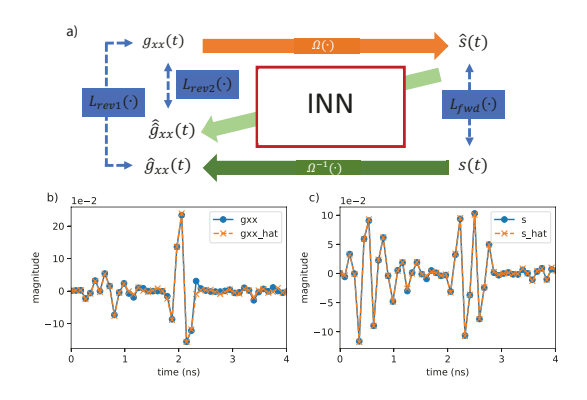


Fig. 1. Illustration of (a) data flow and cost function in INN training, (b) an example of Green's functions  $g_{xx}(t)$  and  $\hat{g}_{xx}(t)$ , and (c) an example of measurements s(t) and  $\hat{s}(t)$ .  $\mathcal{L}_{fwd}(\cdot)$ ,  $\mathcal{L}_{rev1}(\cdot)$ , and  $\mathcal{L}_{rev2}(\cdot)$  represent forward (fwd) and reverse (rev) losses.

The dataset consists of training and testing, with the first (top) layer fixed to have a relative permittivity  $\varepsilon_r^0$  of 13 and a thickness  $d^0$  of 10 mm. The training dataset contains 75,767 tissue profiles  $(g_{xx}(t))$  generated from 2-layer and 3-layer models, and the test dataset contains 18,286 tissue profiles generated from 3-layer and 4-layer models.  $\varepsilon_r^s$ ,  $\varepsilon_r^e$ ,  $d^s$ , and  $d^e$  represent the start and end relative permittivity and thickness for the i'th-layer. The stepsize of relative permittivity and thickness are denoted by  $\Delta \varepsilon_r$  and  $\Delta d$ . The details of the

configuration is given in Table I.  $G_{xx}(\omega)$  and  $S_{12}(\omega)$  are calculated using the frequency range consists with the actual measurements. The time domain passband data  $g_{xx}(t)$  and s(t) are obtained through inverse Fourier transform.

TABLE I SUMMARY OF DATASET

	$\varepsilon_r^s$	$\varepsilon_r^e$	$\Delta \varepsilon_r$	$d^s$	$d^e$	$\Delta d$
Training 2-layer	2.0	21.0	0.025	5.0	50	1.0
Training 3-layer	2.0	21.0	1.0	5.0	50	5.0
Testing 3-layer	2.5	20.5	1.0	7.5	25	5.0
Testing 4-layer	3.5	19.5	3.0	6.0	40	2.0

#### III. INVERTIBLE NEURAL NETWORK (INN)

INN is a family of Artificial Neural Network (ANN) using Normalizing Flow that has been used in image generation and biomedical imaging tasks [5]–[7]. Unlike conventional ANNs, individual components of INNs are fully invertible between input and output.

We construct an INN that contains seven identical blocks where each block contains a sequence of fully invertible operations including affine coupling, permutation, and global affine transformation. In forward path, the INN produces samples from  $p(s(t)|g_{xx}(t))$ , which is identical to a conventional feedforward NN. In reverse path, the INN creates samples from  $p(g_{xx}(t)|s(t))$ . Fig. 1 illustrates the training data flow and loss function design. The invertibility is enforced by regularizing mean squared losses (MSE) in both forward and reverse paths. The forward loss is defined between s(t) and its estimate  $\hat{s}(t)$ , and the reverse loss is defined between  $g_{xx}(t)$  and its estimate  $\hat{g}_{xx}(t)$ . An additional reverse loss is added between  $g_{xx}(t)$  and  $\hat{g}_{xx}(t) = \text{INN}^{-1}(\hat{s}(t))$  to discourage overfitting. The total loss  $\mathcal{L}$  is expressed as follows,

$$\mathcal{L} = \lambda_1 ||s - \hat{s}||^2 + \lambda_2 ||g_{xx} - \hat{g}_{xx}||^2 + \lambda_3 ||g_{xx} - \hat{\hat{g}}_{xx}||^2$$
 (2)

where  $\lambda_{1,2,3}$  are weights of the individual losses.

#### IV. EXPERIMENT SETUP AND RESULTS

#### A. Experiment Setup

We used a PyTorch based FrEIA framework [8] for the INN implementation. The training and testing are performed on a single Nvidia Quadro RTX 6000 GPU and Intel Xeon CPU server. Additive white Gaussian noise (AWGN) is added to s(t) to 40 dB signal to noise ratio (SNR) to improve model generalization capacity and stability. The Adam optimizer with learning rate set to 0.001 is used throughout the training.

# B. Results

Performance of the INN is evaluated by the normalized mean squared error (NMSE), expressed as

NMSE = 
$$\frac{||g_{xx}(t) - \hat{g}_{xx}(t)||^2}{||g_{xx}(t)||^2}$$
(3)

where  $\hat{g}_{xx}(t) = \text{INN}^{-1}[s(t) + n(t)]$ , and n(t) is AWGN. We also provide the lower bound of the NMSE using a genieaided estimator that assumes  $H(\omega)$  and  $H_i(\omega)$  are known. We

evaluate the results from 10 to 80 dB SNR, and the results are presented in Fig. 2.

The results confirm the feasibility of using INNs to recover  $g_{xx}(t)$  from s(t). The model achieves near-optimal performance at SNR regime of 10-30 dB, while there is a gap in the performance at high SNR regime.

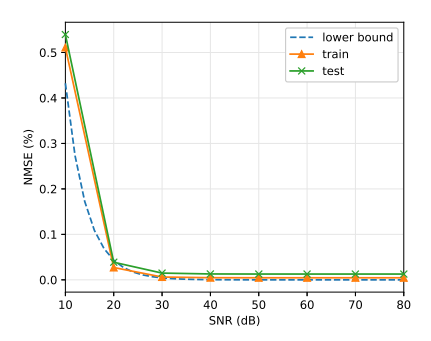


Fig. 2. NMSE of INN estimates  $\hat{g}_{xx}(t)$  from noisy measurements at 10 to 80 dB SNR for profiles in the training and test sets. A lower bound to performance is computed through inversion with known antenna transfer function.

### V. CONCLUSION

We proposed an INN approach for estimating and inverting antenna transfer functions from in situ measurements of multilayer profiles. Our empirical results show that the INN can successfully recover the Green's function of previously unseen multilayer profiles in the testset from noisy measurements. In future work, we will consider inversion of more complex antenna models with feedback. We also plan to investigate near field modeling of returns from 3D tissue profiles and inversion of transfer function of directional patch antennas.

#### **ACKNOWLEDGEMENT**

This research was partially supported by NSF grants CNS1823070 CBET-2037398, and NIH Grant P41EB028242.

## REFERENCES

- B. C. Civek, N. Sugavanam, S. Baskar, and E. Ertin, "Blind deconvolution methods for estimation of multilayer tissue profiles with ultrawideband radar," in 2019 IEEE Radar Conference (RadarConf), 2019, pp. 1–6.
- [2] S. Lambot, E. C. Slob, I. van den Bosch, B. Stockbroeckx, B. Scheers, and M. Vanclooster, "Estimating soil electric properties from monostatic ground-penetrating radar signal inversion in the frequency domain," Water Resources Research, vol. 40, no. 4, 2004.
- [3] S. Lambot, E. Slob, I. van den Bosch, B. Stockbroeckx, and M. Vanclooster, "Modeling of ground-penetrating radar for accurate characterization of subsurface electric properties," *IEEE Transactions on Geoscience* and Remote Sensing, vol. 42, no. 11, pp. 2555–2568, 2004.
- [4] D. J. Griffiths, "Introduction to electrodynamics," 1999.
- [5] D. P. Kingma and P. Dhariwal, "Glow: Generative flow with invertible 1x1 convolutions," in *Advances in Neural Information Processing Systems*, S. Bengio, H. Wallach, H. Larochelle, K. Grauman, N. Cesa-Bianchi, and R. Garnett, Eds., vol. 31. Curran Associates, Inc., 2018.
- [6] I. Kobyzev, S. D. Prince, and M. A. Brubaker, "Normalizing flows: An introduction and review of current methods," *IEEE Transactions on Pattern Analysis amp; Machine Intelligence*, vol. 43, no. 11, pp. 3964–3979, nov 2021.
- [7] A. Denker, M. Schmidt, J. Leuschner, and P. Maass, "Conditional invertible neural networks for medical imaging," *Journal of Imaging*, vol. 7, no. 11, p. 243, 2021.
- [8] L. Ardizzone, T. Bungert, F. Draxler, U. Köthe, J. Kruse, R. Schmier, and P. Sorrenson, "Framework for Easily Invertible Architectures (FrEIA)," 2018-2022.